

## Recent results from NA61/SHINE on spectra and correlations in p+p and Be+Be interactions at the CERN SPS

---

**Andrzej Wilczek\* (for the NA61/SHINE Collaboration)**

*University of Silesia in Katowice, Poland*

*E-mail: [awilczek@us.edu.pl](mailto:awilczek@us.edu.pl)*

The problem of pinning down the critical point of strongly interacting matter still puzzles the community. One of the answers suspected to emerge in the near future will surely come from NA61/SHINE - a fixed-target experiment aiming to discover the critical point as well as to study the properties of the onset of deconfinement.

This goal will be pursued by obtaining precise data on hadron production in proton-proton, proton-nucleus and nucleus-nucleus interactions in a wide range of system size and collision energy.

This contribution presents new results on inclusive spectra of identified hadrons and on fluctuations in inelastic p+p and Be+Be interactions at the SPS energies. These are compared with the world data, in particular with the corresponding measurements of NA49 for central Pb+Pb collisions as well as with some model predictions.

*7th International Conference on Physics and Astrophysics of Quark Gluon Plasma  
1-5 February, 2015  
Kolkata, India*

---

\*Speaker.

## 1. The NA61/SHINE facility

The NA61/SHINE experiment [1] uses a large acceptance hadron spectrometer located in the H2 beam-line at the CERN SPS accelerator complex. The layout of the experiment is schematically shown in Fig. 1. The main detector system is a set of large volume Time Projection Chambers (TPCs). Two of them (VTPC-1 and VTPC-2) are placed inside super-conducting magnets (VTX-1 and VTX-2) with a combined bending power of 9 Tm. The standard current setting for data taking at 158 GeV/c corresponds to full field, 1.5 T, in the first and reduced field, 1.1 T, in the second magnet. For lower beam momenta the field is scaled by  $p_{beam}/158$ , where  $p_{beam}$  is the beam momentum expressed in AGeV/c.

Two large TPCs (MTPC-L and MTPC-R) are positioned downstream of the magnets, symmetrically to the undeflected beam. A fifth small TPC (GAP-TPC) is placed between VTPC-1 and VTPC-2 directly on the beam line and covers the gap between the sensitive volumes of the other TPCs. The NA61/SHINE TPC system allows precise measurement of the particle momenta  $p$  with a resolution of  $\sigma(p)/p^2 \approx (0.3 - 7) \times 10^4 (\text{GeV}/c)^{-1}$  at the full magnetic field used for data taking at 158 GeV/c and provides particle identification via the measurement of the specific energy loss,  $dE/dx$ , with relative resolution of about 4.5%.

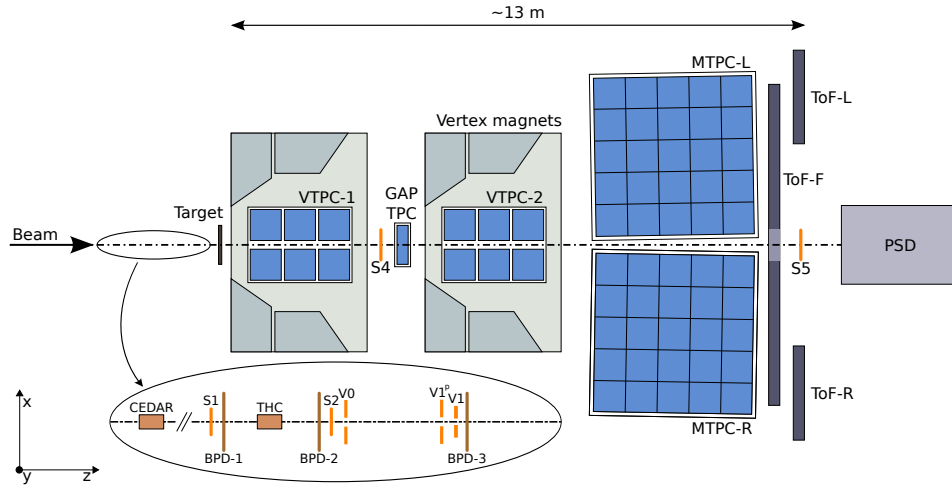


**Figure 1:** Schematic layout of the NA61/SHINE experiment at the CERN SPS (horizontal cut in the beam plane, not to scale). The chosen right-handed coordinate system is shown on the plot. The incoming beam direction is along the  $z$  axis. The magnetic field bends charged particle trajectories in the  $x$ - $z$  (horizontal) plane. The drift direction in the TPCs is along the  $y$  (vertical) axis [1].

A set of scintillation and Cherenkov counters, as well as beam position detectors (BPDs) upstream of the main detection system provide the timing reference, as well as identification and position measurements of the incoming beam particles.

Secondary hadron beams of momentum ranging from 20 to 158 GeV/c are produced by 400 GeV/c primary protons impinging on a 10 cm long beryllium target. Hadrons produced at the target are transported downstream to the NA61/SHINE experiment along the H2 beamline, in which collimation and momentum selection occur. Protons in the secondary hadron beam are iden-

tified by a differential Cherenkov counter (CEDAR). For data taking on  $p+p$  interactions a liquid hydrogen target (LHT) of 20.29 cm length (2.8% interaction length) and 3 cm diameter was placed 88.4 cm upstream of VTPC-1. Inelastic  $p+p$  interactions in the LHT are selected by requiring an anti-coincidence of an identified incoming beam proton with a small scintillation counter of 2 cm diameter (S4) placed on the beam trajectory between the two spectrometer magnets.

Be beams are obtained by fragmentation of primary Pb ions from the SPS in a Be target of 18 cm length. The magnets and collimators of the H2 beam line are set to select a clean  ${}^7\text{Be}$  beam from the fragmentation products. This beam is impinging on a  ${}^9\text{Be}$  plate target of 1.2 cm thickness. Trigger and centrality selection in  ${}^7\text{Be}+{}^9\text{Be}$  interactions were performed using a modular zero-degree calorimeter (Particle Spectator Detector - PSD). The selection is based on the forward energy ( $E_F$ ) deposited in the PSD, which allows to obtain the fraction of total inelastic cross-section by comparing the  $E_F$  deposition with the predictions of the Wounded Nucleon Model.

Data taking with inserted and removed target was alternated in order to calculate a data-based correction for interactions with the material surrounding the target. Further details on the experimental setup, beam and the data acquisition can be found in Ref. [1].

## 2. Reactions and the methods of particle identification

This paper presents results from inelastic  $p+p$  and centrality selected  ${}^7\text{Be}+{}^9\text{Be}$  interactions and compares them with data published by other experiments, including results of Pb+Pb, and Au+Au collisions.

The following methods of particle identification are used for the analyses described in the following sections.

- The  $h^-$  method [2] is used for calculation of  $\pi^-$  spectra. For this method, all negatively charged particles are treated as  $\pi^-$  and a simulation-determined correction factor is applied to account for the small contamination by  $K^-$ ,  $\bar{p}$  and products of weak decays (feed-down).
- Specific energy loss ( $dE/dx$ ) within the active volume of the TPCs is used for identification of charged particles i.e.  $p$ ,  $\bar{p}$ ,  $K^\pm$ , and  $\pi^\pm$  employing a statistical method. The  $dE/dx$  measurements are binned in momentum  $p$  and transverse momentum  $p_T$  of the particles. For each bin a fit is performed to a sum of Gauss functions (one for each particle type). Using the fitted functions, each track is assigned a probability of being a particle of given type. The summed probabilities provide the respective particle multiplicities.
- Time of flight (tof) measurement was combined with  $dE/dx$  information, allowing to separate different kinds of particles in the mid-rapidity region, where the cross-over in specific energy loss is the most significant. The square of the particle mass  $m^2$  is calculated from the particle track length, time of flight, and momentum. The 2-dimensional particle distribution in  $dE/dx$  and  $m^2$  in  $(p, p_T)$  bins is then fitted to 2-dimensional Gaussian distributions and the multiplicities of different particle types are obtained as above.
- $\Lambda$  hyperons are identified using a special pattern finding algorithm to find the  $V^0$ -topology characteristic for their decay. The invariant mass of the outgoing particle pair is calculated under the assumption of  $p$  and  $\pi^-$  masses. The resulting invariant mass distribution for the

appropriate phase-space bin is fitted by a sum of a Lorentz function (signal) and Chebyshev polynomial of 2<sup>nd</sup> order (combinatorial background) to obtain the  $\Lambda$  yield. Acceptance, feed-down, detector and reconstruction efficiency are corrected using simulations.

### 3. Results for p+p interactions

#### 3.1 Observables used as signatures of the onset of deconfinement

The main part of the NA61/SHINE program focuses on the observables sensitive to the phase transition between hadron gas and the quark-gluon plasma (QGP) and the presence of a critical point (CP) of strongly interacting matter. High quality data from p+p reactions presented in this section are a mandatory reference for the measurements involving heavy ions.

One of the signatures predicted for the phase transition is a clear minimum in the energy dependence of the velocity of sound  $c_s$ . This effect is due to the softening of the equation of state (EoS) in the mixed state system of a 1st order phase transition. As the width  $\sigma$  of the rapidity distribution can be expressed by  $c_s$  [3]

$$\sigma^2 = \frac{8}{3} \frac{c_s^2}{1 - c_s^4} \ln(\sqrt{s_{NN}}/2m_N), \quad (3.1)$$

the minimum should be directly visible for the width of  $\pi^-$  rapidity spectra (Fig. 2 left). The minimum is expected only in the case of a transition to the QGP in heavy-ion collisions. Interestingly, such a structure emerges also in p+p collisions (Fig. 2 right).

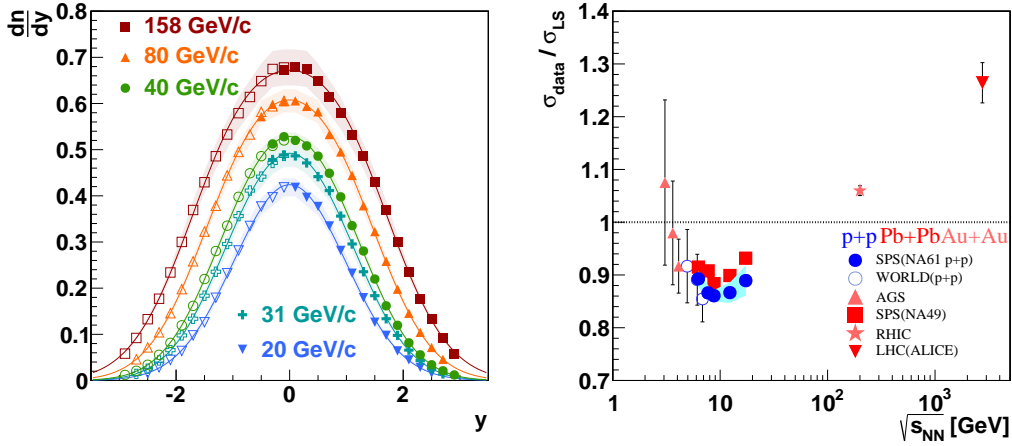


**Figure 2:** Left: rapidity dependence of  $\pi^-$  yields in inelastic p+p interactions for momenta ranging from 20 to 158 GeV/c fitted to a sum of two identical Gauss functions symmetrically displaced from mid-rapidity. Right: data in the width of the rapidity distribution normalised to  $\sigma_{LS}$  (from the Landau-Shuryak hydrodynamic model [3, 4] observed at  $\sqrt{s_{NN}} \approx 10$  GeV. The corresponding minimum of the sound velocity is generally interpreted as softening of the EoS due to creation of a mixed phase at the transition energy from hadrons to partonic matter [5]. Interestingly, this signature is found not only for heavy ion collisions [6, 7, 8], but also for p+p reactions. The results are not corrected for isospin effects.

A signature predicted by the Statistical Model of the Early Stage (SMES) [5] is the ratio of entropy (measured by the multiplicity of pions) to the number of wounded nucleons (interacting

projectile and target nucleons). The SMES model predicts a linear increase with the energy variable  $F = \frac{(\sqrt{s}-2m_p)^{3/4}}{\sqrt{s}^{1/4}}$  [9] for the situation without the phase transition, while the creation of the QGP results in an increase of the slope ('the kink'), because the produced entropy increases due to the activation of the partonic degrees of freedom. The measurement of pion multiplicities in inelastic  $p+p$  interactions at SPS energies and the world data (see Fig. 3) suggest that in fact for  $F > 1$  GeV<sup>1/2</sup> pion production rises linearly, while the data for Pb+Pb, and Au+Au show a significant steepening of the rate of increase of pion production between 40 and 80A GeV/c.

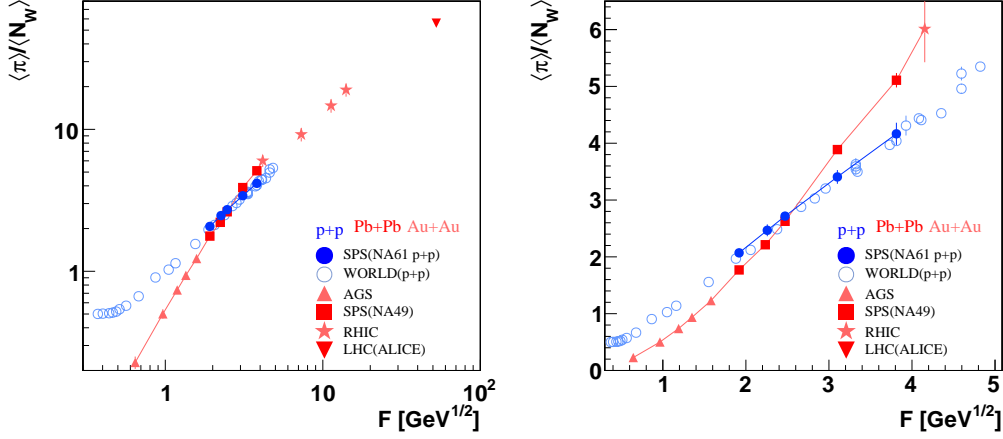


**Figure 3:** Dependence of  $\pi$  multiplicity on the energy variable  $F$  (see text). Also plotted is a compilation of world data based on Ref. [7, 10] including the preliminary NA61/SHINE results on  $p+p$  interactions (solid circles). Double-logarithmic scale (left), linear scale (right).

The second SMES-suggested signature of the onset of QGP production analysed by NA61/SHINE was the centre-of-mass energy  $\sqrt{s_{NN}}$  dependence of the inverse slope parameter  $T$  of the transverse mass  $m_T$  distributions for  $K^\pm$  at mid-rapidity. A stationary behaviour (the 'step') was predicted in the mixed-phase region and actually observed in central Pb+Pb collisions. Surprisingly, the NA61/SHINE results from inelastic  $p+p$  interactions (Fig. 4) also exhibit a 'step' structure like that found in central Pb+Pb collisions.

The most interesting signature is predicted by the SMES in the ratio of strangeness to entropy production. The energy dependence of the related ratio  $\langle K^+ \rangle / \langle \pi^+ \rangle$  is expected to show a rapid increase in the hadron gas phase followed by an abrupt drop at the onset of deconfinement due to a jump in entropy production and then a smooth decrease due to further increase of entropy. This results in the 'horn' structure in heavy-ion collisions, which is not expected in the reference  $p+p$  data, as the transition to the QGP is improbable there. Actually, a step-like structure (precursor of the 'horn') is visible in inelastic  $p+p$  interactions (Fig. 5) motivating a more thorough theoretical study with incorporation of strict strangeness conservation [11].

### 3.2 Strange neutral particles - $\Lambda$

The rapidity spectrum of  $\Lambda$  hyperons from NA61/SHINE is compared in Fig. 6 (left) to results from five bubble-chamber experiments which measured  $p+p$  interactions at beam momenta close

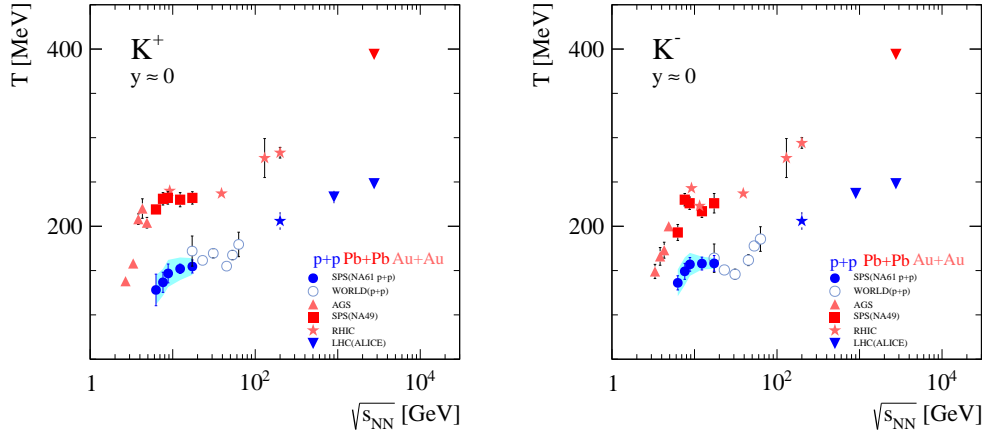


**Figure 4:** Energy dependence of inverse slope parameter  $T$  of kaon transverse mass spectra ( $K^+$  (left),  $K^-$  (right)) showing preliminary NA61/SHINE results on  $p+p$  interactions (solid circles) and a compilation of world data from Ref. [12, 13, 14, 15].

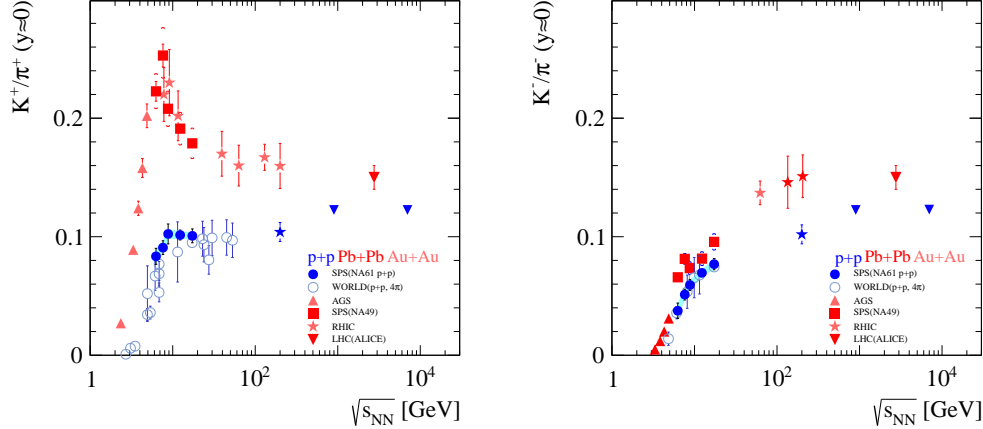


**Figure 5:** Left: the energy dependence of the  $K^+/\pi^+$  ratio in  $p+p$  interactions changes rapidly at the energy where the 'horn' structure is visible in Pb+Pb. Such a behaviour was not predicted in  $p+p$  interactions by models, including the Statistical Model of the Early Stage, which predicted the 'horn' structure as a signature of the Quark-Gluon Plasma (QGP). Right: the energy dependence of the  $K^-/\pi^-$  ratio in  $p+p$  and heavy-ion interactions. The energy dependence of the  $K^-/\pi^-$  ratio does not reveal the horn structure since it is not representative of total strangeness production. The world data plotted in both panels is taken from the Ref. [10, 15, 16, 17, 18].

to 158 GeV/c. The experiments published data for the backward hemisphere, however, with rather small statistics [19, 20, 21, 22, 23] and correspondingly large uncertainties. To account for the difference in beam momentum the spectra are shown in terms of the scaled rapidity  $z = y/y_{beam}$  and were normalised to unity in order to compare the shapes.

Though the statistical error and the systematic uncertainty of the NA61/SHINE measurement is much smaller than for the other experiments, and the results are consistent with all the datasets used for the comparison, the general tendency obtained by fitting a symmetric polynomial of 4<sup>th</sup> order does not describe well the NA61/SHINE data. On the other hand, the result of Brick *et al.* for which the beam momentum (147 GeV/c) differs the least from the NA61/SHINE momentum, shows the best agreement.

The estimated total multiplicity of  $\Lambda$  hyperons produced in inelastic p+p interactions at 158 GeV/c is compared in Fig. 6 (right) with the world data [16] as well as with predictions of the EPOS1.99 model in its validity range. A steep rise in the threshold region is followed by a more gentle increase at higher energies that is well reproduced by the EPOS1.99 model.

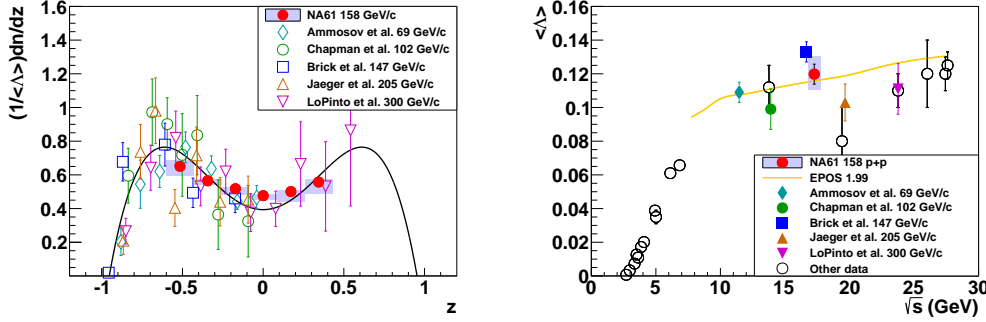


**Figure 6:** *Left:* The  $\Lambda$  yield as function of scaled rapidity  $z = y/y_{beam}$  and normalised to unity in inelastic p+p interactions measured by NA61/SHINE and selected bubble-chamber experiments [19, 20, 21, 22, 23]. The symmetric polynomial of 4<sup>th</sup> order used for estimation of the systematic uncertainty of  $\Lambda$  total multiplicity is plotted to guide the eye. *Right:* Collision energy dependence of total multiplicity of  $\Lambda$  hyperons produced in inelastic p+p interactions. Full symbols indicate bubble chamber results, the solid red dot shows the NA61/SHINE result. Open symbols depict the remaining world data [16]. The prediction of the EPOS1.99 [24] model is shown by the curve. The systematic uncertainty of the NA61/SHINE result is indicated by the shaded bar.

### 3.3 Two-particle $\Delta\eta\Delta\phi$ correlations

The correlation between charged particles in centre-of-mass pseudo-rapidity  $\eta$  and azimuthal angle  $\phi$  was measured by the following 2-particle correlation function:

$$C(\Delta\eta, \Delta\phi) = \frac{N_{mixed}^{pairs}}{N_{single}^{pairs}} \frac{S(\Delta\eta, \Delta\phi)}{M(\Delta\eta, \Delta\phi)}, \quad (3.2)$$

where  $\Delta\eta$  and  $\Delta\phi$  are the rapidity and azimuthal angle difference of the particles and

$$S(\Delta\eta, \Delta\phi) = \frac{d^2 N_{single}^{pairs}}{d\Delta\eta d\Delta\phi}, \quad (3.3)$$



and

$$M(\Delta\eta, \Delta\phi) = \frac{d^2 N_{mixed}^{pairs}}{d\Delta\eta, d\Delta\phi}. \quad (3.4)$$

Here  $N_{single}^{pairs}$  denotes the number of pairs in the events and  $N_{mixed}^{pairs}$  the number of pairs of tracks taken from different events, the latter representing the uncorrelated reference.

The  $\Delta\phi$  range is folded, i.e. for  $\Delta\phi$  larger than  $\pi$  its value is recalculated as  $2\pi - \Delta\phi$ . Detector effects were corrected using simulations and were found to be small.

The results in Fig. 7 (left) show a clear enhancement at  $(\Delta\eta, \Delta\phi)=(0, \pi)$  most likely due to resonance decays and momentum conservation, and a weaker enhancement at  $(\Delta\eta, \Delta\phi)=(0, 0)$  probably due to Coulomb interactions and quantum statistics.

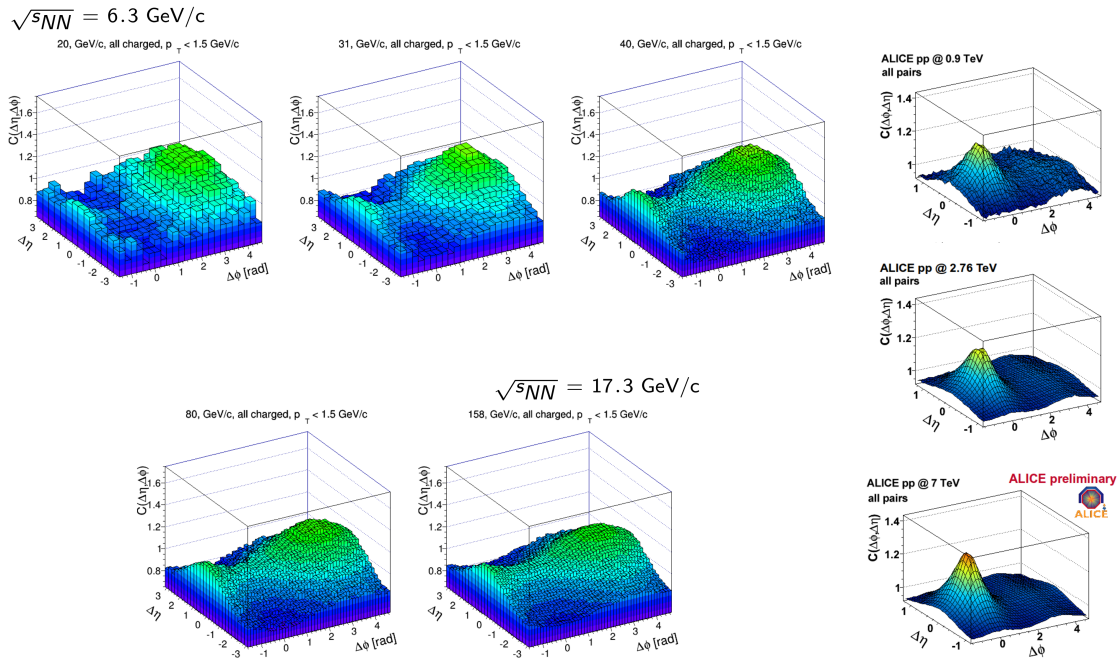


**Figure 7:** Left: Correlation functions  $C(\Delta\eta, \Delta\phi)$  measured by NA61/SHINE show a maximum at  $(\Delta\eta, \Delta\phi)=(0, \pi)$  probably due to resonance decays and momentum conservation. In comparison with the measurement performed at ultra-relativistic energies by ALICE [25] (right), the NA61/SHINE results show a stronger enhancement for  $\Delta\phi \approx \pi$  but no 'jet peak'.

## 4. Results of ${}^7\text{Be}+{}^9\text{Be}$ interactions

### 4.1 Inelastic ${}^7\text{Be}+{}^9\text{Be}$ cross section

The inelastic cross section for  ${}^7\text{Be}+{}^9\text{Be}$  interactions was determined for 13A, 20A, and 30A GeV/c using the pulse-height distributions of the S4 counter - a round scintillator counter of 2 cm in diameter (see Fig. 1). The values measured by the NA61/SHINE experiment (Fig. 8) [26]



are in good agreement with an earlier measurement at lower momentum [27], as well as with the predictions of the Glauber-based Glissando model [28].

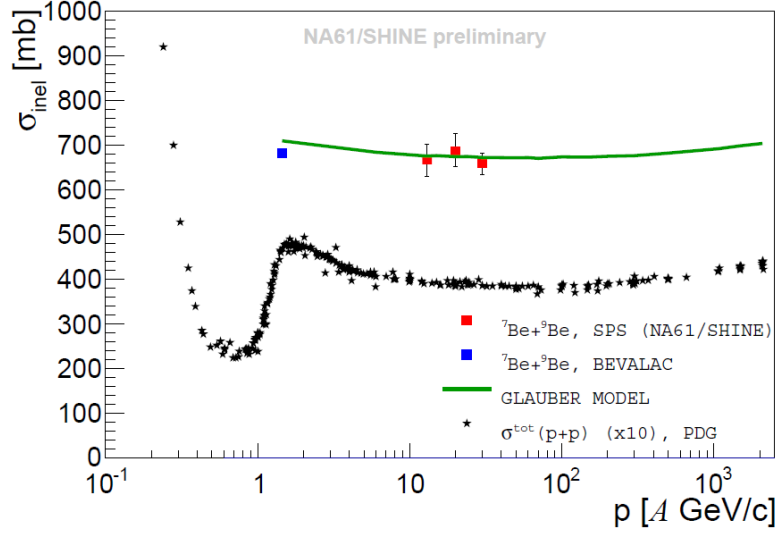


**Figure 8:** Beam momentum dependence of the total inelastic cross section for  ${}^7\text{Be}+{}^9\text{Be}$  interactions. The NA61/SHINE data (red squares), together with the LBNL result (blue square) [27] establish the energy dependence of the cross section. Calculations using the Glissando model [28] are shown by the green curve for comparison.

## 4.2 Rapidity distributions

The  $\pi^-$  rapidity distributions for  ${}^7\text{Be}+{}^9\text{Be}$  collisions at five beam momenta and in four centrality classes together with data for inelastic  $p+p$  interactions are presented in Fig. 9. One observes a small asymmetry about mid-rapidity in the rapidity distributions for  ${}^7\text{Be}+{}^9\text{Be}$  collisions. There are two effects, which may be responsible for this feature. On the one hand, there is a mass asymmetry between projectile ( ${}^7\text{Be}$ ) and target ( ${}^9\text{Be}$ ) nuclei, which is expected to enhance particle production in the backward hemisphere. On the other hand, the selection of central collisions requires a small number of projectile spectators without any restriction imposed on the number of target spectators. For collisions of identical nuclei this would enhance particle production in the forward hemisphere. As the two effects compensate each other to a great extent, the asymmetry of the measured spectra tends to be relatively small. Figure 9 shows that the second effect is a little bit stronger.

## 4.3 Transverse mass distributions

Figure 10 presents the mid-rapidity  $m_T$  spectra of  $\pi^-$  production obtained in the analysis of  ${}^7\text{Be}+{}^9\text{Be}$  collisions at five beam momenta and for four centrality classes and compares them to data for inelastic  $p+p$  interactions as well as to Pb+Pb results of NA49. The spectra are exponential for  $p+p$  reactions but start deviating from this simple shape for collisions of nuclei.

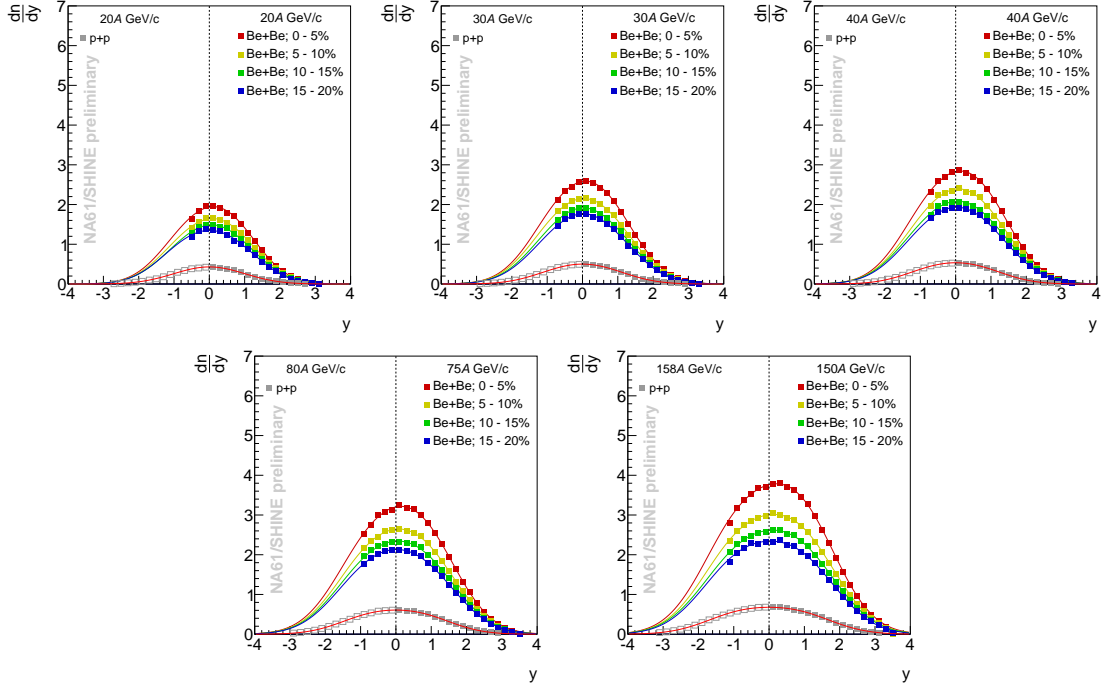


**Figure 9:** Rapidity spectra of  $\pi^-$  in  ${}^7\text{Be}+{}^9\text{Be}$  collisions at 5 beam momenta 20A, 30A, 40A, 75A, and 150A GeV/c for 4 centrality classes compared to  $p+p$  data [2] at the nearest measured energy.

The inverse slope parameter  $T$ , characterising the spectra, was obtained from a fit to the data using the thermal ansatz:

$$\frac{d^2n}{m_T dm_T dy} = A e^{-\frac{m_T}{T}}. \quad (4.1)$$

The dependence of  $T$  on the collision energy (see Fig. 11) for the most central  ${}^7\text{Be}+{}^9\text{Be}$  events was compared with the NA61/SHINE data on  $p+p$  interactions, as well as with the NA49 data on central  $\text{Pb}+\text{Pb}$  collisions. The results for  ${}^7\text{Be}+{}^9\text{Be}$  lie above those for  $p+p$  and below those for  $\text{Pb}+\text{Pb}$  collisions leading to the conclusion that a collective flow effect already starts in central  ${}^7\text{Be}+{}^9\text{Be}$  reactions.

#### 4.4 The quest for the critical point

When the freeze-out of the produced particle system occurs close to the critical point of strongly interacting matter, one should observe a maximum of event-by-event fluctuations. In order to compare the data for different reactions and detector acceptances, the studied observables should be independent of system size and its fluctuations. Therefore, NA61/SHINE measured two strongly intensive measures  $\Delta$  and  $\Sigma$  proposed in Refs. [29, 30].

Preliminary results for charged particles (mainly pions) in four centrality classes of  ${}^7\text{Be}+{}^9\text{Be}$  reactions are shown in Fig. 12 and compared to  $p+p$  data. Consistent with expectations for such small-size systems, no structure is observed in this energy - system size scan that might suggest effects of the critical point.

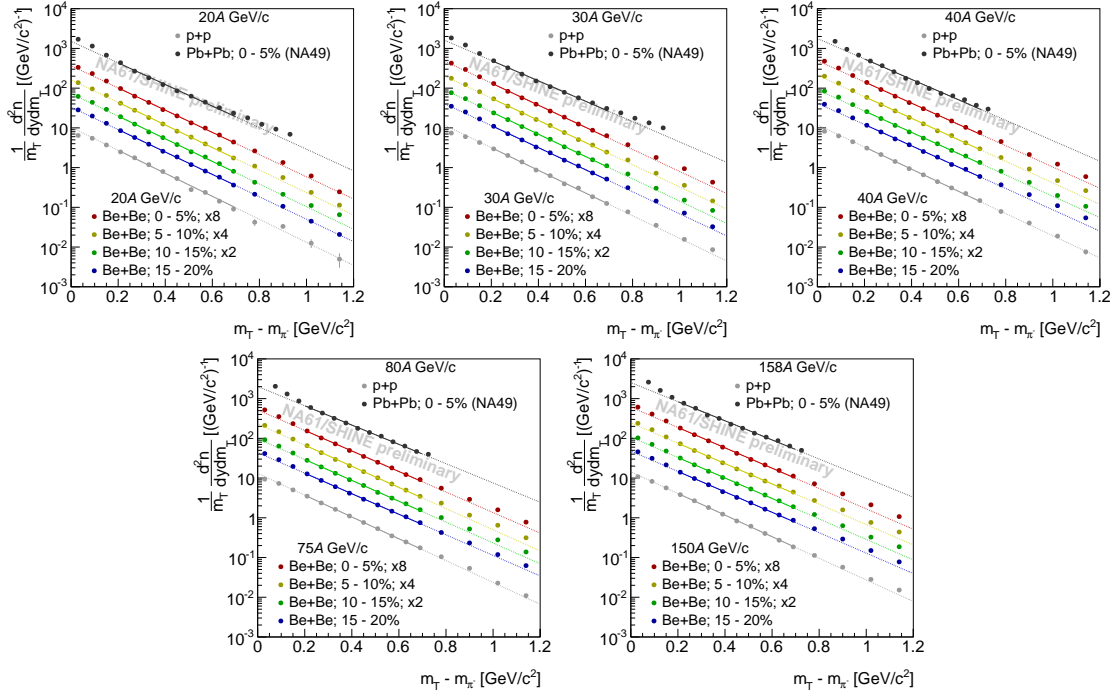


**Figure 10:** Transverse mass spectra of  $\pi^-$  at mid-rapidity in  ${}^7\text{Be}+{}^9\text{Be}$  collisions at 5 beam momenta 20A, 30A, 40A, 75A, and 150A GeV/c for 4 centrality classes compared to  $p+p$  [2] and central  $Pb+Pb$  [31] data at the nearest measured energy.

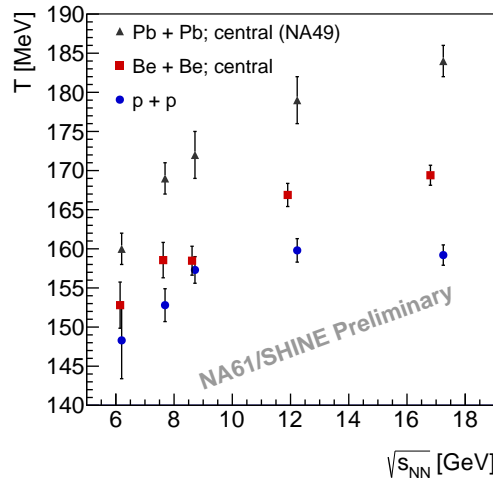


**Figure 11:** Inverse slope parameter  $T$  obtained from  $\pi^-$  transverse mass distributions at mid-rapidity for  $p+p$  [2] and central  ${}^7\text{Be}+{}^9\text{Be}$  and  $Pb+Pb$  [31] collisions. The high inverse slope parameter in  $Pb+Pb$  interactions is due to radial flow. The values of  $T$  for  ${}^7\text{Be}+{}^9\text{Be}$  are between those of  $p+p$  and  $Pb+Pb$  collisions and can be interpreted as possible evidence of transverse collective flow in central  ${}^7\text{Be}+{}^9\text{Be}$  interactions. Note: the fitted inverse slope parameter  $T$  in  $A+A$  collisions is sensitive to the fit range and the location of the rapidity bin.

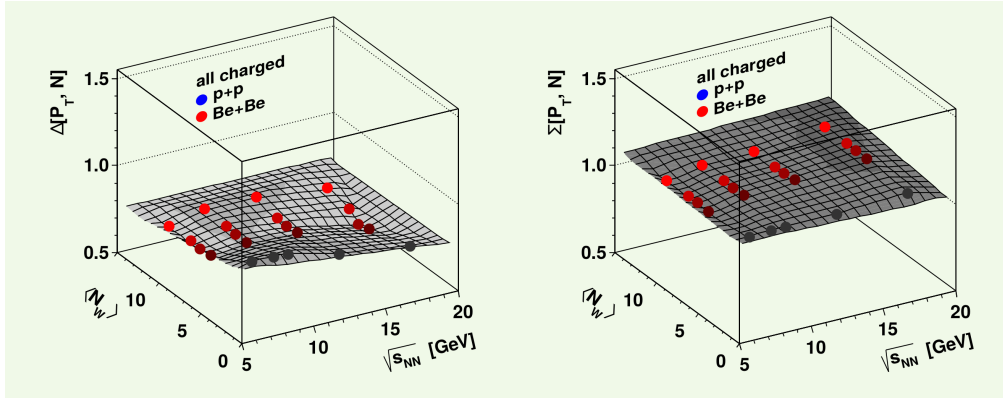


**Figure 12:** The critical point of strongly interacting matter is expected to cause a maximum of fluctuations of hadronic observables. No sign of such an anomaly is observed for  $\Delta$  and  $\Sigma$  in either  $p+p$  or  ${}^7\text{Be}+{}^9\text{Be}$  collisions. The plotted measures  $\Delta$  and  $\Sigma$  of transverse momentum fluctuations are strongly intensive, thus independent of the system volume and its fluctuations.

## 5. Summary

The NA61/SHINE experiment at the CERN SPS is a unique facility which operates with various primary and secondary beams (hadrons, ions) interacting with stationary targets.

The scientific program of the experiment covers three main fields of interest: reference measurements for neutrino physics and cosmic ray experiments, as well as studies of hadron interactions at beam momenta needed to reach the onset of deconfinement and the critical point of strongly interacting matter. In addition, cold nuclear matter effects are investigated in proton-nucleus interactions.

The ongoing NA61/SHINE scan program covers a wide range of beam energies and collision system sizes. First results from  $p+p$  and  ${}^7\text{Be}+{}^9\text{Be}$  collisions are presented in this paper.

High precision double-differential pion spectra were measured at five different energies for both systems. In  $p+p$  reactions the energy dependence of the  $K^+/\pi^+$  and  $K^-/\pi^-$  ratios and of the inverse slope parameter  $T$  of the transverse mass spectra of kaons were determined. The results for  $K^+$  show rapid changes with collision energy, even for inelastic  $p+p$  interactions. These structures resemble similar effects observed in central  $\text{Pb}+\text{Pb}$  interactions at SPS energies.

Collective flow effects are observed already in  ${}^7\text{Be}+{}^9\text{Be}$  collisions.

No sign for the critical point of strongly interacting matter was found for these small-sized systems.

## Acknowledgements

This work was supported by the Hungarian Scientific Research Fund (grants OTKA 68506 and 71989), the János Bolyai Research Scholarship of the Hungarian Academy of Sciences, the Polish Ministry of Science and Higher Education (grants 667/N-CERN/2010/0, NN 202 48 4339 and NN 202 23 1837), the Polish National Science Centre (grants **2011/03/N/ST2/03691**, 2012/

04/M/ST2/00816 and 2013/11/N/ST2/03879), the Foundation for Polish Science — MPD program, co-financed by the European Union within the European Regional Development Fund, the Federal Agency of Education of the Ministry of Education and Science of the Russian Federation (SPbSU research grant 11.38.193.2014), the Russian Academy of Science and the Russian Foundation for Basic Research (grants 08-02-00018, 09-02-00664 and 12-02-91503-CERN), the Ministry of Education, Culture, Sports, Science and Technology, Japan, Grant-in-Aid for Scientific Research (grants 18071005, 19034011, 19740162, 20740160 and 20039012), the German Research Foundation (grant GA 1480/2-2), the EU-funded Marie Curie Outgoing Fellowship, Grant PIOF-GA-2013-624803, the Bulgarian Nuclear Regulatory Agency and the Joint Institute for Nuclear Research, Dubna (bilateral contract No. 4418-1-15/17), Ministry of Education and Science of the Republic of Serbia (grant OI171002), Swiss Nationalfonds Foundation (grant 200020117913/1) and ETH Research Grant TH-01 07-3. Finally, it is a pleasure to thank the European Organisation for Nuclear Research for strong support and hospitality and, in particular, the operating crews of the CERN SPS accelerator and beam lines who made the measurements possible.

## References

- [1] N. Abgrall *et al.* [NA61 Collaboration], JINST **9** (2014) P06005 [arXiv:1401.4699 [physics.ins-det]].
- [2] N. Abgrall *et al.* [NA61/SHINE Collaboration], Eur. Phys. J. C **74** (2014) 3, 2794 [arXiv:1310.2417 [hep-ex]].
- [3] L. D. Landau, Izv. Akad. Nauk Ser. Fiz. **17** (1953) 51.
- [4] E. V. Shuryak, IYF-75-4.
- [5] M. Gaździcki, M. Gorenstein and P. Seyboth, Acta Phys. Polon. B **42** (2011) 307 [arXiv:1006.1765 [hep-ph]].
- [6] J. L. Klay *et al.* [E-0895 Collaboration], Phys. Rev. C **68** (2003) 054905 [nucl-ex/0306033].
- [7] E. Abbas *et al.* [ALICE Collaboration], Phys. Lett. B **726** (2013) 610 [arXiv:1304.0347 [nucl-ex]].
- [8] S. S. Adler *et al.* [PHENIX Collaboration], Phys. Rev. C **69** (2004) 034909 [nucl-ex/0307022].
- [9] E. Fermi, Prog. Theor. Phys. **5** (1950) 570.
- [10] B. Abelev *et al.* [ALICE Collaboration], Phys. Rev. Lett. **109** (2012) 252301 [arXiv:1208.1974 [hep-ex]].
- [11] R. V. Poberezhnyuk, M. Gaździcki and M. I. Gorenstein, arXiv:1502.05650 [nucl-th].
- [12] M. Kliemant, B. Lungwitz and M. Gaździcki, Phys. Rev. C **69** (2004) 044903 [hep-ex/0308002].
- [13] B. I. Abelev *et al.* [STAR Collaboration], Phys. Rev. C **79** (2009) 034909 [arXiv:0808.2041 [nucl-ex]].
- [14] B. B. Abelev *et al.* [ALICE Collaboration], Phys. Lett. B **736** (2014) 196 [arXiv:1401.1250 [nucl-ex]].
- [15] K. Aamodt *et al.* [ALICE Collaboration], Eur. Phys. J. C **71** (2011) 1655 [arXiv:1101.4110 [hep-ex]].
- [16] M. Gaździcki and D. Röhrich, Z. Phys. C **71** (1996) 55 [hep-ex/9607004].
- [17] M. Gaździcki and D. Röhrich, Z. Phys. C **65** (1995) 215.
- [18] I. Arsene *et al.* [BRAHMS Collaboration], Phys. Rev. C **72** (2005) 014908 [nucl-ex/0503010].

- [19] V.V. Ammosov et al., Nucl. Phys. B **115**, (1976) 269
- [20] J.W. Chapman et al., Phys.Lett. **47B**, (1973) 465
- [21] D. Brick et al., Nucl. Phys. B **164**, (1980) 1
- [22] K. Jaeger et al., Phys. Rev. D **11**, (1975) 2405
- [23] F. LoPinto et al., Phys. Rev. D **22**, (1980) 573
- [24] K. Werner, F.-M. Liu, and T. Pierog, Phys. Rev. C **74** (2006) 044902
- [25] M. Janik, PoS WPCF **2011** (2011) 026 [arXiv:1203.2844 [hep-ex]].
- [26] I. Weimer, <https://edms.cern.ch/file/1308546>
- [27] I. Tanihata *et al.*, Phys. Rev. Lett. **55** (1985) 2676.
- [28] W. Broniowski, M. Rybczynski and P. Bozek, Comput. Phys. Commun. **180** (2009) 69 [arXiv:0710.5731 [nucl-th]].
- [29] M. I. Gorenstein and M. Gaździcki, Phys. Rev. C **84** (2011) 014904 [arXiv:1101.4865 [nucl-th]].
- [30] M. Gaździcki, M. I. Gorenstein and M. Maćkowiak-Pawłowska, Phys. Rev. C **88** (2013) 2, 024907 [arXiv:1303.0871 [nucl-th]].
- [31] S. V. Afanasiev *et al.* [NA49 Collaboration], Phys. Rev. C **66** (2002) 054902 [nucl-ex/0205002].